Structural Engineering and Mechanics, *Vol. 59, No. 6 (2016) 1071-1094*
DOI: http://dx.doi.org/10.12989/sem.2016.59.6.1071

Problem-dependent cubic linked interpolation for Mindlin plate four-node quadrilateral finite elements

Dragan Ribarić*

Faculty of Civil Engineering, University of Rijeka, R. Matejčić 3, 51000 Rijeka, Republic of Croatia

(Received April 6, 2016, Revised June 14, 2016, Accepted June 15, 2016)

Abstract. We employ the so-called problem-dependent linked interpolation concept to develop two cubic 4-node quadrilateral plate finite elements with 12 external degrees of freedom that pass the constant bending patch test for arbitrary node positions of which the second element has five additional internal degrees of freedom to get polynomial completeness of the cubic form. The new elements are compared to the existing linked-interpolation quadratic and nine-node cubic elements presented by the author earlier and to the other elements from literature that use the cubic linked interpolation by testing them on several benchmark examples.

Keywords: Mindlin plate theory; quadrilateral displacement-based plate finite elements; problem-independent and problem-dependent linked interpolation

1. Introduction

The concept of a *linked interpolation*, in which the displacement field depends not only on the nodal displacements, but also on the nodal rotations, has been largely exploited in the numerical simulations for the Mindlin-plate finite-element models (Zienkiewicz and Taylor 2000, Jelenić and Papa 2011, Zienkiewicz *et al.* 1993, Taylor and Auricchio 1993, Xu *et al.* 1994, Auricchio and Taylor 1994, Ribarić and Jelenić 2012). When used with no other provisions, the linked intepolation as the only plate problem interpolation, applied on the general quarlilateral element with 4 nodes is able to pass the constant bending patch test exactly (Jelenić and Papa 2011). This test is acctualy considered as the main consistence crtiteria for the convergence of a finite element model, but passing the test on its own does not mean that the convergence is at the same time acceptably fast (Chen *et al*. 2009).

By "quadratic" linked interpolation we here mean such interpolation in which the displacement field is described by a linear interpolation of the nodal displacements onto which a quadratic interpolation of the nodal rotations is superimposed. At the same time the rotation fields are interpolated bilinearly (Lagrangean) and all interpolations are controled by 4+4 rotational degrees of freedom and 4 nodal displacement degrees of freedom. Since the element displacement and the rotations are interpolated independently, in deriving the element deformations and stress resultants only the first derivatives of the displacement and rotation fields are needed.

*Corresponding author, Ph.D., E-mail: dragan.ribaric@uniri.hr

http://www.techno-press.org/?journal=sem&subpage=8 ISSN: 1225-4568 (Print), 1598-6217 (Online)

Many reasurchers have used the linked interpolation as a basis for developing their new plate elements and have found that the linked interpolation by itself is not sufficient for development of well-behaving finite elements, so they have attempted to improve it by introducing additional ideas (Hughes and Tezduyar 1981, NacNeal 1982, Crisfield 1984, Bathe and Dvorkin 1986 among others)

Tessler and Dong (1981) introduced a *shear constraint condition* to eliminate free internal nodal degrees of freedom in the Timoshenko's beam higher-order displacement and rotation interpolations, as a better approach than the static condensation of those degrees of freedom. Inspired by this idea, Tessler and Hughes (1983) used *continuous transverse shear edge constraints* on serendipity 8-node displacement and 4-node rotation interpolations to derive *a non-uniform order kinematic interpolation scheme* (here called the linked interpolation). Additional requirements on total strain energy were adopted to improve the rate of convergence by introducing what was termed the *element-appropriate shear correction factors*.

The low-order quadratic linked interpolation, together with added higher order terms in the rotation interpolations and a mixed-type approach involving interpolation of the shear force field, were proposed by Zienkiewicz *et al*. (1993), Taylor and Auricchio (1993, 1994), Xu *et al*. (1994) in order to improve the accurcy of the plate model as well as to satisfy the necessary count conditions of the mixed-type approach.

Crisfield (1984) started with a nine-node Lagrangian interpolation for the displacement field and an eight-node serendipity interpolation for the rotation fields and constructed a pure *displacement-based* plate element where some of the internal degrees of freedom were again eliminated by the use of *shear constraints*. The resulting element had twelve vertex degrees of freedom and four pairs of independent rotation degrees of freedom at the element side midpoints. In the present paper, the idea of Crisfield (1984) is developed further, and these midside rotations are going to be replaced by the projections of the normal-to-the-side hierarhical rotations together with additional bubble-type rotations needed to complete the quadratic rotation interpolation form.

In his paper, Ibrahimbegović (1993) used the quadratic and the cubic linked interpolations to construct two parent types of elements as we do in the present work, but with shear strain independently assumed to take a linear interpolation form. He also leaves the hierarhical midside normal rotations as independent variables between adjacent elements and studies only undistorted element meshes. The same concept but with triangular elements was studied by Papadopoulos and Taylor (1990).

Wanji and Cheung (2000) used a similar approach with the cubic linked interpolation, but they eliminated the midside rotations by constraining shear to be constant along the element sides. This allowed both the displacement and the rotation field to be expressed using only the boundary degrees of freedom, but came with the expense of introducing the material constants in the interpolation, which thus became problem-dependent (Dukić and Jelenić 2014) and linked not only in the displacement, but also in the rotation field. Shear strain was then assumed as an independent field and interpolated between the opposite element sides. Using identical displacement expressions as Wanji and Cheung (2000), Zhang and Kuang (2007) developed a nine-node element with improved results.

Soh *et al*. (2001) took a similar approach, but expressed shear using nodal shear values derived from shear strains of adjacent sides to the regarded node. All their elements (*RDKQM* (Wanji and Cheung 2000) and *ARS-Q12* (Soh *et al.* 2001)) derived using the cubic interpolation and the assumed shear concept showed excellent behaviour for regular and distorted meshes in the numerical tests.

More elements with excellent performance can be found among the hybrid-Trefftz plate elements of Choo *et al*. (2010), Rezaiee-Pajand and Karkon (2012) (*QHT*), Cen *et al*. (2014) (*HDF-P4-11β*), who also used the cubic linked interpolation as an element side constraint for the fundamental analytical solution of the displacement function by witch the deflection and rotation fields can be expressed. The unknown coefficients of the displacement function are determined by satisfying generalized conforming conditions on the element sides in terms of the nodal parameters.

In Ribarić and Jelenić (2012) the linked interpolation is expanded from the four node quadrilaterals to the higher order elements (nine- and sixteen-node elements) increasing the interpolation polynomial order, resulting in the increased accuracy and faster convergence rates, while remaining strictly within the realm of the pure displacement approach. Since higher-order polynomials employed there to construct higher-order linked-interpolation elements resulted in significaly better finite-element performance, here we want to answer to the question of whether it is posible to use higher-order poynomials with the same result on lower-order elements. In particular, we shall investigate if four-node qudrilateral elements may be improved by increasing the order of the linked interpolation from quadratic to cubic.

2. Linked interpolations on four-node plate element

The key ingredients of the Minlin plate theory involving kinematic and constitutive equations as well as the weak form are given in Zienkiewicz and Taylor (2000). In Ribarić and Jelenić (2012) the following linked interpolation for the transverse displacement field *w* along with two standard Lagrangian interpolations for the rotations around the global co-ordinate axes have been proposed for the lowest-order linked-interpolation element *Q4-U2*

$$\theta_{x(Q4-U2)} = \frac{1-\xi}{2}\frac{1-\eta}{2}\theta_{x,1} + \frac{1+\xi}{2}\frac{1-\eta}{2}\theta_{x,2} + \frac{1+\xi}{2}\frac{1+\eta}{2}\theta_{x,3} + \frac{1-\xi}{2}\frac{1+\eta}{2}\theta_{x,4} \tag{1a}$$

$$\theta_{y(Q4-U2)} = \frac{1-\xi}{2}\frac{1-\eta}{2}\theta_{y,1} + \frac{1+\xi}{2}\frac{1-\eta}{2}\theta_{y,2} + \frac{1+\xi}{2}\frac{1+\eta}{2}\theta_{y,3} + \frac{1-\xi}{2}\frac{1+\eta}{2}\theta_{y,4} \tag{1b}$$

$$\begin{aligned} w_{(Q4-U2)} = {} & \frac{1-\xi}{2}\frac{1-\eta}{2}w_1 + \frac{1+\xi}{2}\frac{1-\eta}{2}w_2 + \frac{1+\xi}{2}\frac{1+\eta}{2}w_3 + \frac{1-\xi}{2}\frac{1+\eta}{2}w_4 \\ & + \frac{1-\xi^2}{4}\frac{1-\eta}{2}\frac{1}{2}\left[\left(\theta_{y2}-\theta_{y1}\right)\left(x_2-x_1\right)-\left(\theta_{x2}-\theta_{x1}\right)\left(y_2-y_1\right)\right] \\ & + \frac{1-\xi^2}{4}\frac{1+\eta}{2}\frac{1}{2}\left[\left(\theta_{y3}-\theta_{y4}\right)\left(x_3-x_4\right)-\left(\theta_{x3}-\theta_{x4}\right)\left(y_3-y_4\right)\right] \\ & + \frac{1+\xi}{2}\frac{1-\eta^2}{4}\frac{1}{2}\left[\left(\theta_{y3}-\theta_{y2}\right)\left(x_3-x_2\right)-\left(\theta_{x3}-\theta_{x2}\right)\left(y_3-y_2\right)\right] \\ & + \frac{1-\xi}{2}\frac{1-\eta^2}{4}\frac{1}{2}\left[\left(\theta_{y4}-\theta_{y1}\right)\left(x_4-x_1\right)-\left(\theta_{x4}-\theta_{x1}\right)\left(y_4-y_1\right)\right] \\ & + \frac{1-\xi^2}{4}\frac{1-\eta^2}{4}w_{B0}\,. \end{aligned} \tag{1c}$$

In this basic linked interpolation for a four-node quadrilateral element, the complete second-order polynomial expansion is involved in interpolating displacement over the element domain (9 items in Pascal's triangle). All existing nodal parameters $w_1,\ldots,w_4$, $\theta_{x1},\ldots,\theta_{x4}$, $\theta_{y1},\ldots,\theta_{y4}$, are involved together with the extra internal parameter w_{B0}. The *Q4-U2* element obtained in this way is capable of passing the standard patch test for general constant bending state exactly. We can describe such an interpolation form as full "quadratic". Conformity with adjacent elements is fulfilled along every element side where interpolations are expressed only by the nodal degrees of freedom (d.o.f.) of that particular side and where the shear strain along the side is constant and also expressed by the same d.o.f. (shear strain continuity).

In Ribarić and Jelenić (2012) it has been also shown how such an approach may be generalised to design a higher-order element *Q9-U3* involving full cubic interpolation of the displacement field (and quadratic interpolation of the rotation fields). This generalisation builds on the interpolation concept termed in Jelenić and Papa (2011) the *problem-independent linked interpolation*, which, when applied to plates, necessarily invloves additional degrees of freedom inside the element and on its sides. In the case of beams, the same solution may be obtained alternatively, using the approach termed in Dukić and Jelenić (2014) the *problem-dependent interpolation* in which (i) the rotational field becomes linked to the nodal displacements, (ii) the shape functions become dependent on the geometric and material properties of the cross section and, very importantly, (iii) both fields are completely defined in terms of only the boundary nodal degrees of freedom. In this work, such a problem-dependent linked interpolation will be generalised to plates in order to develop new four-node elements *Q4-U3* and assess their performance against the problem-independent linked-interpolation nine-node element *Q9-U3* of the same order given in Dukić and Jelenić (2014).

Following the complete Timoshenko beam homogeneous solution (see Appendix A) and generalising it to plate elements, interpolations along the element side can take a full form (cubic in displacement and quadratic in rotations), in which conformity along the element sides is still

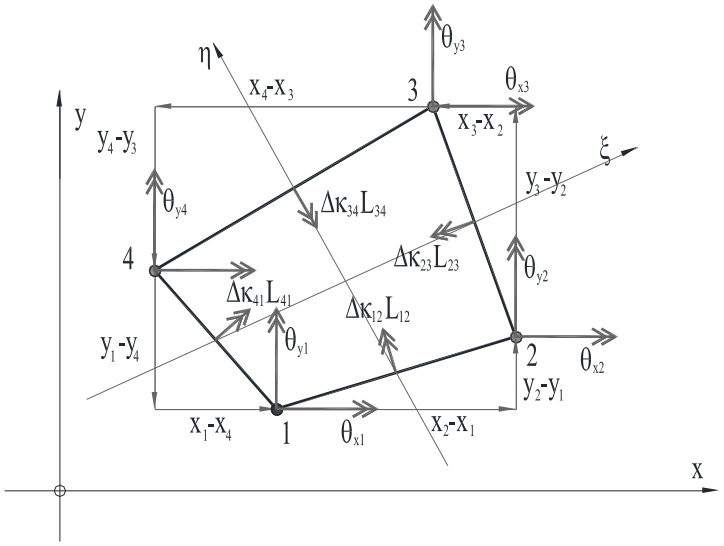

Fig. 1 Vectors of the nodal rotations (d.o.f.), and vectors of the normal-to-the-side hierarchical rotations

preserved together with the shear strain continuity, constraining shear along the element side to be constant again. In this way we obtain

$$\theta_{x(Q4\text{–}U3)} = \theta_{x(Q4\text{–}U2)} - \frac{1-\xi^2}{4}\frac{1-\eta}{2}\Delta\kappa_{12}(y_2-y_1) - \frac{1+\xi}{2}\frac{1-\eta^2}{4}\Delta\kappa_{23}(y_3-y_2)$$
$$-\frac{1-\xi^2}{4}\frac{1+\eta}{2}\Delta\kappa_{34}(y_4-y_3) - \frac{1-\xi}{2}\frac{1-\eta^2}{4}\Delta\kappa_{41}(y_1-y_4) \tag{2a}$$

$$\theta_{y(Q4\text{–}U3)} = \theta_{y(Q4\text{–}U2)} + \frac{1-\xi^2}{4}\frac{1-\eta}{2}\Delta\kappa_{12}(x_2-x_1) + \frac{1+\xi}{2}\frac{1-\eta^2}{4}\Delta\kappa_{23}(x_3-x_2)$$
$$+\frac{1-\xi^2}{4}\frac{1+\eta}{2}\Delta\kappa_{34}(x_4-x_3) + \frac{1-\xi}{2}\frac{1-\eta^2}{4}\Delta\kappa_{41}(x_1-x_4) \tag{2b}$$

$$w_{(Q4\text{–}U3)} = w_{(Q4\text{–}U2)} - \frac{\xi-\xi^3}{4}\frac{1-\eta}{2}\Delta\kappa_{12}\frac{L_{12}^2}{6} - \frac{1+\xi}{2}\frac{\eta-\eta^3}{4}\Delta\kappa_{23}\frac{L_{23}^2}{6}$$
$$+\frac{\xi-\xi^3}{4}\frac{1+\eta}{2}\Delta\kappa_{34}\frac{L_{34}^2}{6} + \frac{1-\xi}{2}\frac{\eta-\eta^3}{4}\Delta\kappa_{41}\frac{L_{41}^2}{6}. \tag{2c}$$

In expressions (2a), (2b) and (2c) the "$\Delta\kappa_{ij}$" are the element side curvature increments per side lengths, added to the global coordinate rotations as hierarchical projections of the normal midside rotations (Fig. 1) and expressed by nodal d.o.f. of that side (see Appendix A)

$$\Delta\kappa_{ij} = -\left(w_j - w_i - \frac{\theta_{xi}+\theta_{xj}}{2}\cdot(y_j-y_i) + \frac{\theta_{yi}+\theta_{yj}}{2}\cdot(x_j-x_i)\right)\frac{1}{1+\dfrac{12D}{L_{ij}^2(Gtk)}}\frac{6}{L_{ij}^2}\cdot \tag{3}$$

Or, for the first side of the element connecting node 1 with node 2

$$\Delta\kappa_{12} = -\left(w_2 - w_1 - \frac{\theta_{x1}+\theta_{x2}}{2}\cdot(y_2-y_1) + \frac{\theta_{y1}+\theta_{y2}}{2}\cdot(x_2-x_1)\right)\frac{1}{1+\dfrac{12D}{L_{12}^2(Gtk)}}\frac{6}{L_{12}^2}\cdot \tag{3.1}$$

In above expressions D is a plate bending rigidity, $D=Et^3/(12(1-\nu^2))$, L_{ij} is the length of the side between the nodes i and j and a plate shear rigidity is Gtk (E and G being the elasticity and shear modulus, ν being the Poisson coefficient, t a plate thickness and k shear section correction factor, usually taken k=5/6).

Following the same approach as in Ribarić and Jelenić (2012) a new plate element named *Q4-U3* is developed based on the existing element *Q4-U2* with interpolation polynomials of an order higher by one - namely (2a), (2b) and (2c). This implementation does not affect the ability of the element to pass the constant bending patch test, because all the side curvature increments $\Delta\kappa_{ij}$, will vanish, as the shear strains along the element side vanish in the patch test. Better behaviour and faster convergence is expected since higher interpolation polynomial forms are involved even though the total number of the degrees of freedom remains unaltered.

Further, more polynomial terms can be added to the interpolation functions, to fulfill the quadratic form for both rotations (one additional term per rotation, missing in the Pascal's triangle), and the cubic form in displacement interpolation (additional three terms missing in the Pascal's triangle for cubic form), all associated to additional new bubble degrees of freedom. In

this way we obtain

$$\theta_{x(Q4-U3R5)} = \theta_{x(Q4-U3)} - \frac{1-\xi^2}{4}\frac{1-\eta^2}{4}\theta_{x,B1} \tag{4a}$$

$$\theta_{y(Q4-U3R5)} = \theta_{y(Q4-U3)} + \frac{1-\xi^2}{4}\frac{1-\eta^2}{4}\theta_{y,B2} \tag{4b}$$

$$w_{(Q4-U3R5)} = w_{(Q4-U3)} + \frac{\xi-\xi^3}{4}\frac{1-\eta^2}{4}\frac{1}{3}w_{B3} + \frac{1-\xi^2}{4}\frac{\eta-\eta^3}{4}\frac{1}{3}w_{B4} + \frac{\xi-\xi^3}{4}\frac{\eta-\eta^3}{4}\frac{1}{3}w_{B5}. \tag{4c}$$

The plate element formulated in this way as an improvement of the cubic linked-interpolation element *Q4-U3* is denoted as *Q4-U3R5*.

Additional terms in (4a), (4b) and (4c) do not affect the ability of the element to pass the constant bending patch test, because all the added bubble functions satisfy the element stiffness matrix criteria from Ribarić (2012) resulting in zero bubble parameters when applied on the patch test, including the bubble functions added in the rotation fields. Also, any of the above five bubble functions can be added individually improving the element behavior to some extent, but the best result is achieved by adding them all, as can be seen in the following numerical results.

3. Numerical examples

In the following numerical experiments the new developed elements *Q4-U3* and *Q4-U3R5* are compared with the already presented elements with the linked interpolations in Ribarić and Jelenić (2012): *Q4-U2* (four-node element with quadratic interpolations) and *Q9-U3* (nine-node element with cubic interpolations) and with the mixed element *Q4-LIM* of Auricchio and Taylor (1994), which also uses the linked interpolation in modeling displacement and rotation fields and is incorporated in their FEAP program. The 3x3 integration scheme is used to form the element stiffness matrix of *Q4-U2* and *Q4-LIM*, while 4x4 is used for *Q4-U3* and *Q4-U3R5* elements. When the sampling point is needed in calculation of the stress resultants, for example in calculation of the extreme values for bending moments, the same points are used, with the exception for *Q4-LIM* element, where the central Gauss integration point is used by the program FEAP.

The expressions for the shear strains derived in *Q4-U3* and *Q4-U3R5* elements have cubic forms, including terms that are responsible for over stiffening of the element matrix and the locking effect for very thin models in coarse meshes. When the reduced integration of the shear terms in presented elements is preformed, with 3×3 integration points, the results are slightly better in all numerical examples. With 2×2 integration points a numerical instability is observed.

The results for the selected numerical examples are also compared with the results of other elements and from the data taken from the referenced literature, when they are comparable in mesh geometry or material data.

3.1 The constant bending patch test

Consistency of the linked interpolation elements is tested for the constant strain conditions on the patch examples with five elements, covering a rectangular domain of a plate as shown in Fig. 2

and Fig. 3. The displacements and rotations for all internal nodes within the patch are checked for the specific displacements and rotations given at all external nodes (Chen *et al.* 2009). The plate properties are $E=10^5$, $v=0.25$, $k=5/6$, while two different thicknesses corresponding to a thick and a thin plate extremes are considered: $t=1.0$ and $t=0.01$.

The constant bending state is analysed (Chen *et al.* 2009). Displacements and rotations are expressed respectively by

$$w=(1+x+2y+x^2+xy+y^2)/2\,,\quad \theta_x=(2+x+2y)/2 \quad \text{and} \quad \theta_y=-(1+2x+y)/2\,.$$

The exact displacements and rotations at the internal nodes and the exact strains and stress resultants at every integration point are expected. The moments are constant $M_x=M_y=$-11111.11 t^3, $M_{xy}=$-3333.33 t^3 and the shear stress resultants vanish ($S_x=S_y=0$).

For the given values for the displacements and rotations at the external nodes calculated from the above data (12 parameters), the displacements and rotations at the internal nodes, the bending and torsional moments and the shear stress resultants at the integration points and the problem strain energy are computed and checked if they correspond to the analytical values.

The results of the patch tests for all proposed elements are given in Table 1 for the displacement at node 1 with coordinates (0.04, 0.02) and for the strain energy of the problem. When exact, the results are not altered if any of the internal nodes changes its position in the mesh.

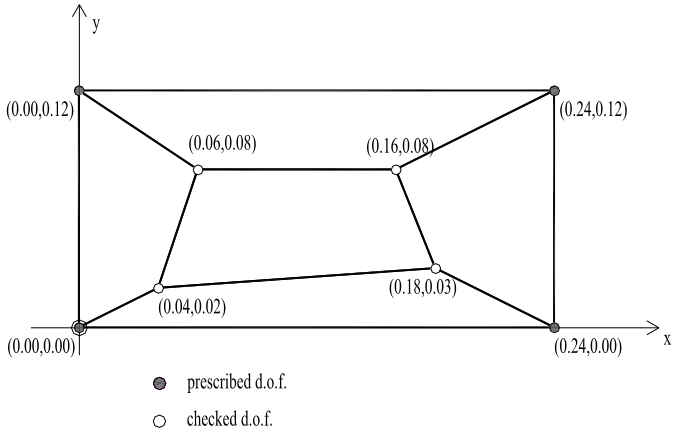

Fig. 2 Patch for consistency assessment of four node elements

Table 1 The patch test results for the proposed elements on the patch geometry from Fig. 2 and Fig. 3, for zero constant shear patch test-constant curvature

Elements	Displacement at node 1 of the patch		Strain energy		Result
	t=1.0	t=0.01	t=1.0	t=0.01	
Q4-LIM	0.5414021	0.5414002	0.3679993E+03	0.3679998E-03	close pass
Q4-U2	0.5414000	0.5414000	0.3680000E+03	0.3680000E-03	pass
Q4-U3	0.5414000	0.5414000	0.3680000E+03	0.3680000E-03	pass
Q4-U3R5	0.5414000	0.5414000	0.3680000E+03	0.3680000E-03	pass
Analytical	0.5414	0.5414	0.3680000E+03	0.3680000E-03	

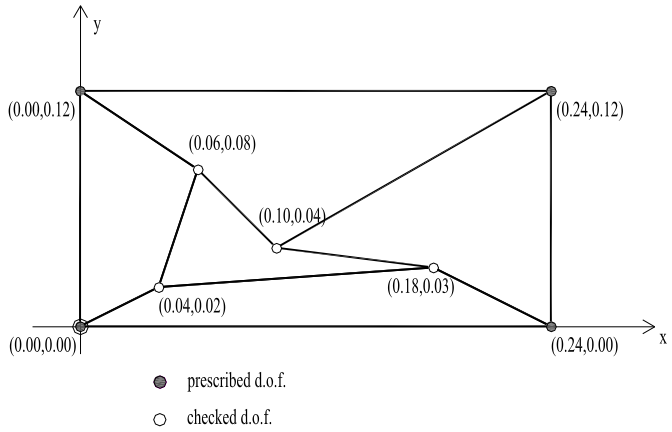

Fig. 3 Element patch for consistency assessment of four node elements with convex distortion and negative Jacobian determinant at some element integration points

Table 2(a) Eigenvalues of a central element in the patch test from Fig. 2, for t=1.0

Element	1	2	3	4	5	6
	7	8	9	10	11	12
Q4-LIM	6.6693E+04	2.7748E+04	1.8138E+04	1.6697E+04	8.3345E+03	5.7079E+03
	4.0838E+03	3.2616E+03	8.8782E+00	-6.6265E-12	-3.3583E-12	-1.0851E-12
Q4-U2	6.6728E+04	2.7795E+04	1.8138E+04	1.6710E+04	8.3345E+03	6.4810E+03
	4.0838E+03	3.7063E+03	8.8820E+00	-5.1792E-12	-2.1934E-12	6.6293E-13
Q4-U3	6.6678E+04	2.7832E+04	1.8138E+04	1.6664E+04	8.3028E+03	6.4753E+03
	4.0838E+03	3.7038E+03	8.8778E+00	-2.5676E-12	-1.0974E-12	1.8844E-13
Q4-U3R5	6.6678E+04	2.7832E+04	1.8138E+04	1.6663E+04	8.3028E+03	5.7076E+03
	4.0838E+03	3.2686E+03	8.8778E+00	-6.7442E-12	3.9096E-12	-1.9294E-12

When the patch test is passed, the elements are not sensitive to the position of the vertex nodes, even if an element has a negative determinant of the Jacobian transformation matrix in some integration point, like some of the elements in Fig. 3 have.

The eigenvalues of the central element from the patchwork of Fig. 2 are calculated next. First a regular form (distortion level 0) of the element is analyzed (with the free internal nodes: (0.06, 0.03), (0.16, 0.03), (0.06, 0.08) and (0.16, 0.08)) together with three different plate thicknesses t=1.0, t=0.01 and t=0.0001, corresponding to the very thick, thin and extremely thin plates. Then the eigenvalues are calculated for the distorted central element shown in Fig. 3, again with the same three different thicknesses. The eigenvalues are given in Tables 2 and 3.

In all cases the elements have the correct rank and only the three eigenvalues, corresponding to the solid body motions are zero. There are no additional spurious zero modes responsible for instability of the finite element models. The eigenvalues for the very thick elements belong to a relatively small subset of real numbers, in regular or distorted geometry thus giving a better conditioned problem. The eigenvalues are getting smaller as the plate thickness is reduced and the better performances can be expected for the elements with eigenvalues in greater proportion to the thickness.

Table 2(b) Eigenvalues of a central element in the patch test from Fig. 2, for t=0.01

Element	1	2	3	4	5	6
	7	8	9	10	11	12
Q4-LIM	9.5984E+01	3.7956E+01	1.4638E+01	3.0158E-02	1.8138E-02	5.7085E-03
	4.6884E-03	4.0838E-03	3.2617E-03	1.1999E-14	-2.6063E-15	1.5871E-15
Q4-U2	6.6727E+02	2.7792E+02	1.6709E+02	1.4201E-01	4.0729E-02	1.8138E-02
	8.7957E-03	5.2137E-03	4.0838E-03	3.5312E-14	2.0054E-14	5.7841E-15
Q4-U3	7.5721E+01	6.4926E+01	5.1823E+00	2.0214E-01	2.0760E-02	1.8930E-02
	1.8138E-02	4.3624E-03	4.0838E-03	8.0639E-14	5.7082E-15	-1.3211E-15
Q4-U3R5	7.5721E+01	6.4926E+01	5.1823E+00	2.0760E-02	1.8138E-02	1.5550E-02
	8.6580E-03	4.3624E-03	4.0838E-03	7.5043E-14	-2.7079E-15	2.6460E-15

Table 2(c) Eigenvalues of a central element in the patch test from Fig. 2, for t=0.0001

Element	1	2	3	4	5	6
	7	8	9	10	11	12
Q4-LIM	1.1211E-04	7.3477E-05	1.6044E-05	3.6279E-08	1.8138E-08	5.7085E-09
	4.8160E-09	4.0838E-09	3.2617E-09	6.6332E-21	-3.6242E-21	1.3526E-21
Q4-U2	6.6727E+00	2.7792E+00	1.6709E+00	1.3889E-03	3.7027E-04	2.3153E-05
	1.8138E-08	5.3307E-09	4.0838E-09	5.7369E-16	-2.7128E-16	1.5136E-16
Q4-U3	1.5904E-01	2.2222E-03	1.3890E-04	8.5385E-05	7.9337E-05	5.3466E-06
	1.8138E-08	5.3295E-09	4.0838E-09	-5.5884E-16	6.9793E-18	1.3609E-18
Q4-U3R5	1.5904E-01	8.5423E-05	7.9337E-05	2.4695E-05	1.2356E-05	5.3455E-06
	1.8138E-08	5.3295E-09	4.0838E-09	-5.5382E-16	7.4190E-18	-4.9468E-18

Table 3(a) Eigenvalues of an irregular central element in the patch test from Fig. 3, for t=1.0

Element	1	2	3	4	5	6
	7	8	9	10	11	12
Q4-LIM	7.2803E+04	3.0391E+04	1.9800E+04	1.4848E+04	8.9441E+03	6.2422E+03
	4.2385E+03	3.0221E+03	1.0143E+01	-3.7733E-12	2.2417E-12	-9.9541E-13
Q4-U2	7.3241E+04	3.1327E+04	1.9811E+04	1.4505E+04	9.0171E+03	7.0887E+03
	4.4838E+03	3.2068E+03	1.0724E+01	5.7283E-12	2.7508E-12	1.1753E-12
Q4-U3	7.3178E+04	3.1379E+04	1.9811E+04	1.4481E+04	8.9441E+03	7.0791E+03
	4.4802E+03	3.2065E+03	1.0730E+01	-3.9317E-12	3.6111E-12	-1.1807E-12
Q4-U3R5	7.3172E+04	3.1047E+04	1.9802E+04	1.4471E+04	8.8804E+03	6.3678E+03
	4.2471E+03	3.0327E+03	1.0645E+01	-6.7439E-12	2.3665E-12	-1.5341E-12

3.2 Cylindrical bending of simply supported strip

In this numerical test the ability of the linked interpolation elements to model constant shear stress state is checked, when the regular element mesh is applied, which corresponds to the orientation of the cylindrical linear bending (Fig. 4). The same test was performed in Auricchio

Table 3(b) Eigenvalues of an irregular central element in the patch test from Fig. 3, for t=0.01

Element	1	2	3	4	5	6
	7	8	9	10	11	12
Q4-LIM	9.0171E+01	3.3633E+01	1.0707E+01	3.3586E-02	1.9798E-02	6.4333E-03
	4.2690E-03	4.1803E-03	3.0219E-03	1.6081E-14	-2.5197E-15	-1.0114E-18
Q4-U2	7.3239E+02	3.1324E+02	1.4502E+02	1.9604E-01	6.3482E-02	1.9837E-02
	1.0173E-02	4.7120E-03	3.6416E-03	2.2270E-14	-8.4562E-15	5.3577E-15
Q4-U3	1.3317E+02	1.0045E+02	1.0045E+02	2.7533E-01	4.0928E-02	1.9640E-02
	1.0477E-02	4.2408E-03	3.6246E-03	8.8104E-15	-3.6379E-15	9.3347E-17
Q4-U3R5	9.8129E+01	7.5352E+01	4.1124E+00	2.7194E-02	2.2634E-02	1.9121E-02
	8.9980E-03	4.1655E-03	3.6241E-03	1.2018E-14	5.0270E-15	-2.7670E-15

Table 3(c) Eigenvalues of an irregular central element in the patch test from Fig. 3, for t=0.0001

Element	1	2	3	4	5	6
	7	8	9	10	11	12
Q4-LIM	1.0350E-04	6.5769E-05	1.1522E-05	3.9015E-08	1.9799E-08	6.4418E-09
	4.3298E-09	4.2190E-09	3.0219E-09	6.2238E-21	-2.8074E-21	-6.5979E-22
Q4-U2	7.3239E+00	3.1324E+00	1.4502E+00	1.9212E-03	5.9407E-04	2.7647E-05
	1.9645E-08	4.9200E-09	3.6480E-09	3.0867E-16	-1.3298E-16	-5.1774E-17
Q4-U3	1.0063E+00	3.6560E-01	3.0024E-02	2.7299E-03	3.8814E-05	2.8545E-06
	1.9644E-08	4.9177E-09	3.6480E-09	-1.0681E-15	-1.2556E-17	-1.6159E-18
Q4-U3R5	3.9180E-01	2.6470E-01	8.1248E-03	3.7637E-05	3.1985E-06	4.1845E-08
	1.9643E-08	4.8561E-09	3.6465E-09	-9.8346E-16	-2.7539E-17	-5.3689E-19

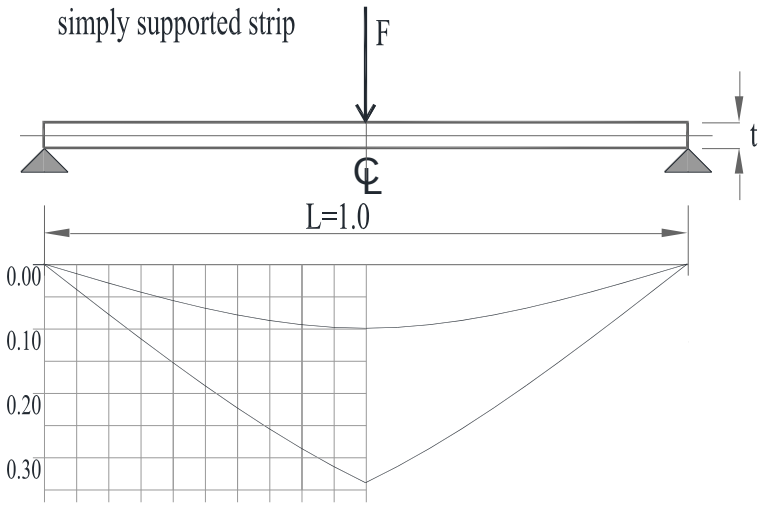

Fig. 4 Simply supported plate strip under symmetric force load, F=400. Vertical displacement for the strip with shear energy included (lower line) and without shear energy (upper line), for t/L=1

Table 4(a) The simply supported strip results for linear bending from Fig. 4 (non-zero constant shear test), displacement at the center, $w_{tot}=w_b+w_s$

Mesh	*Q4-LIM*		*Q4-U2*		*Q4-U3* and *Q4-U3-R5*	
	t=1.0	t=0.01	t=1.0	t=0.01	t=1.0	t=0.01
1×2	0.33352	0.93543E+05	0.315000	0.75024E+05	0.34000	1.00024E+05
1×4	0.33880	0.98825E+05	0.333750	0.93774E+05	0.34000	1.00024E+05
1×10	0.33983	0.99853E+05	0.339000	0.99024E+05	0.34000	1.00024E+05
1×50	0.33999	1.0002E+05	0.339960	0.99984E+05	0.34000	1.00024E+05
1×100	0.34000	1.0002E+05	0.339990	1.00014E+05	0.34000	1.00024E+05
Exact	0.34000	1.00024E+05	0.34000	1.00024E+05	0.34000	1.00024E+05

Table 4(b) The simply supported strip results for linear bending from Fig. 4 (non-zero constant shear test), total energy of the model, $E_{tot}=E_b+E_s$

Mesh	*Q4-LIM*		*Q4-U2*		*Q4-U3* and *Q4-U3-R5*	
	t=1.0	t=0.01	t=1.0	t=0.01	t=1.0	t=0.01
1×2	1.334074E+02	3.741701E+07	1.260000E+02	3.000960E+07	1.360000E+02	4.000960E+07
1×4	1.355202E+02	3.952980E+07	1.335000E+02	3.750960E+07	1.360000E+02	4.000960E+07
1×10	1.359317E+02	3.994127E+07	1.356000E+02	3.960960E+07	1.360000E+02	4.000960E+07
1×50	1.359973E+02	4.000693E+07	1.359840E+02	3.999360E+07	1.360000E+02	4.000960E+07
1×100	1.359993E+02	4.000893E+07	1.359960E+02	4.000560E+07	1.360000E+02	4.000960E+07
Exact	1.360000E+02	4.000960E+07	1.360000E+02	4.000960E+07	1.360000E+02	4.000960E+07

and Taylor, 1994 and none of the elements tested there could pass the test when elements of finite size were used. Here all cubic elements, the *Q4-U3* and *Q4-U3R5* are capable to reproduce the analytical solution exactly with only two elements in the mesh for any thickness (see Tables 4(a) and 4(b)). The material properties are: E=1000, v=0.0.

It is interesting to notice that in this example all five bubble terms in *Q4-U3R5* turn out to be zero by the imposed equilibrium conditions, so the parameters engaged are equal to the parameters in *Q4-U3*.

Furthermore, when distributed load is applied, the cubic interpolated plate elements give exact results for transverse nodal displacement and rotation in every node and close approximations for the moment and shear resultants in every integration point and for the total strain energy. In fact, the solution exact at nodes will be obtained for any type of loading, as described by Tong (see Zienkiewicz and Taylor 2000 and Appendix A).

3.3 Simply supported square plate with regular meshes

A square plate with simply supported edges is a standard test example in which displacements and nodal rotations around the normal on the model edge are set to zero (*SS2* support condition) and plate is subjected to a central point force of magnitude P=100.0. The plate material properties are E=10.92 and v=0.3. Because of the double symmetry only one quarter of the plate is modeled and appropriate boundary conditions are imposed on the symmetry lines (Fig. 5). All elements in the model are regular (distortion of the level 0 in Ribarić and Jelenić 2014) and the rate of

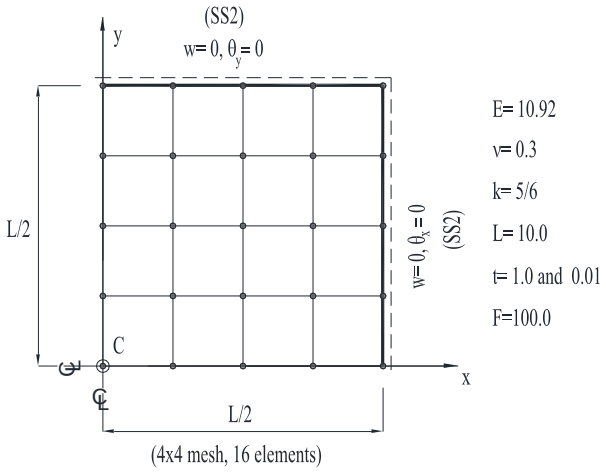

Fig. 5 A quarter of the square plate under central point force at point *C* (16-element mesh)

Table 5 Simply supported square plate (SS2) with the central point force: the displacement (w^*) at the center

Element	*L/t*	Element mesh density						Reference
		2×2	4×4	8×8	16×16	32×32	64×64	
Q4-U2		1.13428	1.27851	1.34276	1.38407	1.41847	1.45082	
Q4-U3		1.24314	1.31198	1.35179	1.38667	1.41923	1.45104	
Q4-U3R5	10	1.25911	1.31202	1.35218	1.38685	1.41928	1.45106	no reference
Q4-LIM		1.24682	1.31092	1.35238	1.38688	1.41928	1.45105	
Q9-U3		1.32542	1.36876	1.40309	1.43531	1.46700	1.49856	
Q4-U2		0.43610	1.03267	1.14118	1.15777	1.16148	1.16266	
Q4-U3		0.26088	0.85562	1.13375	1.16066	1.16245	1.16290	
Q4-U3R5	100	0.92408	1.13560	1.15899	1.16177	1.16245	1.16291	no reference
Q4-LIM		1.11040	1.14605	1.15740	1.16103	1.16230	1.16289	
Q9-U3		1.11724	1.15606	1.16142	1.16260	1.16310	1.16345	
Q4-U2		0.07686	0.14280	0.80227	1.11913	1.15584	1.15954	
Q4-U3		0.00499	0.04031	0.35006	0.99598	1.14518	1.15901	
Q4-U3R5	1000	0.05123	0.47876	1.05075	1.13704	1.15926	1.16003	1.160 (Kirchhoff solution)
Q4-LIM		1.10901	1.14435	1.15540	1.15874	1.15972	1.16000	
Q9-U3		1.03422	1.12816	1.15492	1.15935	1.16001	1.16010	

convergence is tested. The results are given in Table 5 for three different span-to-thickness ratios.

In the table, dimensionless transverse displacement $w^*=w/(PL^2/100D)$ is given. As the moment at the center should theoretically reach infinity and the model has singularity at the center point, it challenges the tested elements in the neighborhood to the center point. The best behavior and the greatest bending moment is reached again by the new *Q4-U3R5* element, with some advantage even to the full cubic interpolated element *Q9-U3*.

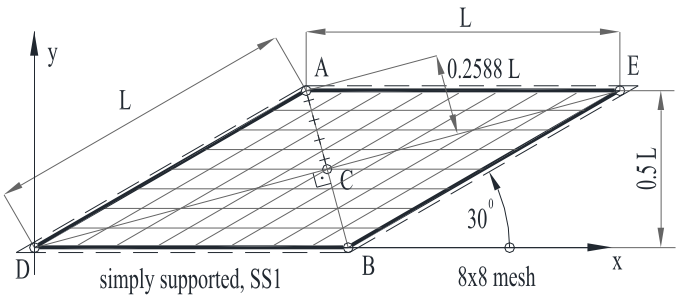

Fig. 6 A simply supported (SS1) skew plate under uniform load

Table 6 Simply supported skew plate: displacement $w^*=w/(qL^4/100D)$ at the center with regular meshes for span to thickness ratio, L/t=100 and L/t=1000

Element	L/t	Element mesh density							Reference
		4×4	8×8	16×16	32×32	48×48	96×96	144×144	
Q4-U2		0.1629	0.2917	0.3745	0.4054	0.4133	0.4203	0.4223	
Q4-U3		0.3118	0.3855	0.4044	0.4119	0.4152	0.4200	0.4221	
Q4-U3R5		0.3397	0.4030	0.4147	0.4171	0.4183	0.4213	0.4229	
Q4-LIM		0.4257	0.4210	0.4231	0.4262	0.4278	0.4294	0.4299	
RDKQM	100	0.757	0.504	0.441	0.423				0.423*
ARS-Q12		0.7535	0.5033	0.4402	0.4230				
HDF-P4-11β		0.463	0.427	0.421	0.420				
QHT		0.425	0.413	0.414	0.416				
Q9-U3		0.3297	0.3872	0.4090	0.4155	0.4218	0.4241		
Q4-U2		0.0094	0.0810	0.2030	0.3136	0.3535	0.3873	0.3969	
Q4-U3		0.1444	0.2624	0.3473	0.3824	0.3930	0.4028	0.4058	
Q4-U3R5		0.1507	0.2684	0.3523	0.3890	0.4000	0.4085	0.4102	
Q4-LIM		0.4185	0.4094	0.4073	0.4080	0.4090	0.4109	0.4119	
RDKQM	1000	0.760	0.507	0.443	0.424				0.408*
ARS-Q12		0.7563	0.5059	0.4424	0.4243				
HDF-P4-11β		0.462	0.426	0.419	0.416				
QHT		0.422	0.409	0.408	0.408				
Q9-U3		0.2425	0.3105	0.3567	0.3740	0.3927	0.4034		

*Reference results are from Zienkiewicz *et al*. (1993)

3.4 Simply supported skew plate

In this example the uniformly load rhombic plate with very sharp skew angle of 30° is

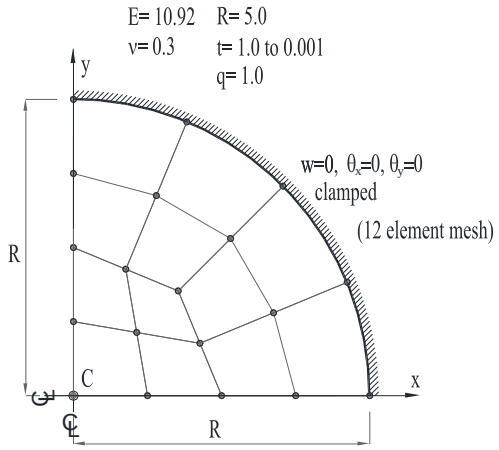

Fig. 7 A quarter of the circular clamped plate under a uniform load (12-element mesh)

considered with the simply supported edges (this time, of the so-called soft type *SS1*) to test performance of the rhombic shaped elements. Since there is a singularity in the moment field at the obtuse angle vertex, this test example is a difficult one. Furthermore, the Morley's series solution (Tessler and Hughes 1983) reveals that moments around the principal directions near that vertex have opposite signs.

The problem geometry and material properties are given in Fig. 6, where an example of an 8×8-element mesh is shown.

The same elements as before are tested and the results are given in Table 6, together with some elements from literature: *Q4-LIM* (Auricchio and Taylor 1994), *Q4-U2* and *Q9-U3* (Ribarić and Jelenić 2012), *RDKQM* (WanJi and Cheung 2000), *ARS-Q12* (Soh *et al.* 2001), QHT (Rezaiee-Pajand and Karkon 2012) and *HDF-P4-11β* (Cen *et al.* 2014), for the thick and the thin plate, respectively. The dimensionless result $w^*=w/(qL^4/10^4D)$, is related to the central displacement of the plate.

Very good result can be observed for the proposed elements on both the thick and the thin plate model.

3.5 Clamped circular plate

In this example the proposed elements will be tested on problems which necessarily involve irregular meshes like the one shown in the Fig. 7. In this example the reference solution can be found analytically and the amount of error in particular field can be evaluated for various mesh densities. The plate is loaded by a uniformly distributed loading q=1.0. The material properties are the same as in the previous examples.

The exact solution for the transverse displacement and the radial rotation of the problem can be derived in polar coordinates (Wang *et al.* 2000) and these results consist of the bending part ("*B*") and the shear part ("*S*"). The index "*M*" stands for the total (Mindlin) expressions

$$w^M = w^B + w^S = \frac{qR^4}{64D}\left\{\left(\frac{r}{R}\right)^4 - 2\left(\frac{r}{R}\right)^2 + 1\right\} + \frac{qR^2}{4kGt}\left[1-\left(\frac{r}{R}\right)^2\right] \tag{5}$$

$$\theta_r^M = \theta_r^B = -\frac{\partial w^B}{\partial r} = \frac{qR^3}{16D}\left(\frac{r}{R}\right)\left\{1-\left(\frac{r}{R}\right)^2\right\}. \tag{6}$$

The total strain energy of the problem is

$$E^M = E^B + E^S = \frac{1}{2}\int_A \boldsymbol{\kappa}^T \mathbf{M} dA + \frac{1}{2}\int_A \boldsymbol{\Gamma}^T \mathbf{S} dA = \frac{1}{2}\left(\frac{q^2R^6\pi}{192D} + \frac{q^2R^4\pi}{8kGt}\right). \tag{9}$$

Again only one quarter of the plate is modeled with appropriate boundary conditions along the chosen axes of symmetry. On the outer boundary clamped state is simulated by enforcing all nodal d.o.f. to be zero. The results are given in Table 7 for all element types and typical meshes and mesh densities used in the literature. A 12-element mesh is depicted in Fig. 7. The dimensionless values of the central point displacement is presented in Table 7:

$$w_c^* = \frac{w_c}{q}\frac{100D}{(2R)^4} \quad \text{with} \quad D = \frac{Et^3}{12(1-\nu^2)}.$$

In Table 7 the influence of different number of bubble terms used in the interpolation functions for the enrichment of the basic *Q4-U3* element is also investigated. When only first two bubble terms in rotation fields (4a) and (4b) are employed the results are given as the *Q4-U3R2* element. When other two bubble terms from (4c) are added in displacement field the results are given as the *Q4-U3R4* element. When all bubble terms are used then the *Q4-U3R5* element is obtained and tested.

The rate of convergence towards the exact solution may be evaluated by calculating error measure of the strain energy for the finite element solution ($\mathbf{u}_h$) compared to the strain energy of the reference solution ($\mathbf{u}_r$)

$$EM(\mathbf{u}_r, \mathbf{u}_h) = \frac{1}{2}\int_A \boldsymbol{\varepsilon}_r{}^T \mathbf{C}\boldsymbol{\varepsilon}_r dA - \frac{1}{2}\int_A \boldsymbol{\varepsilon}_h{}^T \mathbf{C}\boldsymbol{\varepsilon}_h dA = E_r - E_h. \tag{10}$$

In this expression $\boldsymbol{\varepsilon}_r$ and E_r denote the reference strain and the reference strain energy (for the clamped circular plate it is the analytical solution (9)), while $\boldsymbol{\varepsilon}_h$ and E_h are the strain and the strain energy from the finite element solution, respectively. **C** denotes the constitutive matrix.

It is often more convenient to analyse the relative error measure:

$$RE(\mathbf{u}_r, \mathbf{u}_h) = \frac{EM(\mathbf{u}_r, \mathbf{u}_h)}{E(\mathbf{u}_r)} = \frac{E_r - E_h}{E_r}. \tag{11}$$

The error measure for the 2D elements with four nodes is proportional to the square of the element density (1/*N*) (Lee and Bathe 2010)

$$EM(\mathbf{u}_r, \mathbf{u}_h) \cong c\left(\frac{1}{N}\right)^2,$$

where *N* is the number of elements per model side and *c* is a constant. The coefficient $\left(\frac{1}{N}\right)^2$ will be the reference measure for comparing the convergence behavior of the presented elements as well as the reference measure for comparison with the results from literature – see Fig. 8 where both values are logarithmically scaled.

Table 7 Clamped circular plate: displacement w_c* at the plate center

Element	2*R/t*	Mesh density (number of the elements in a mesh)					Reference
		3	12	48	192	768	
Q4-U2		0.0806344	0.1063609	0.1132119	0.1149365	0.1153693	
Q4-U3		0.0894061	0.1094969	0.1139128	0.1150988	0.1154087	
Q4-U3R2		0.0929097	0.1095449	0.1139429	0.1151128	0.1154127	
Q4-U3R4		0.0931750	0.1095478	0.1139432	0.1151128	0.1154127	
Q4-U3R5		0.0930929	0.1095479	0.1139436	0.1151129	0.1154127	
Q4-LIM	10	0.09160	0.11063	0.11533	0.11649	0.11678	0.1155134
RDKQM		0.12303	0.11748	0.11604			
ARS-Q12		0.123434	0.117584	0.115989	0.115629		
HDF-P4-11β		0.09472	0.10988	0.11402	0.11513		
QHT		0.0946	0.1099	0.1140			
Q9-U3		0.1155342	0.1155166	0.1155128	0.1155133		
Q4-U2		0.0187898	0.0747157	0.0944037	0.0971967	0.0976901	
Q4-U3		0.0059686	0.0497918	0.0910725	0.0972421	0.0977428	
Q4-U3R5		0.0576750	0.0900175	0.0963267	0.0974890	0.0977468	
Q4-LIM		0.073635	0.091985	0.096406	0.097490	0.097760	
RDKQM	100	0.107709	0.100793	0.098695			0.0978348
ARS-Q12		0.107685	0.100781	0.0985873	0.0980133		
HDF-P4-11β		0.07812	0.09279	0.09657	0.09752		
QHT		0.0777	0.0928	0.0966			
Q9-U3		0.0969626	0.0978155	0.0978339	0.0978348		
Q4-U2		0.0002611	0.0047363	0.0438103	0.0899167	0.0970286	
Q4-U3		0.0000649	0.0021103	0.0214904	0.0753062	0.0953238	
Q4-U3R2		0.0004593	0.0068514	0.0490272	0.0912598	0.0971433	
Q4-U3R4	1000	0.0010042	0.0251863	0.0816792	0.0962204	0.0975028	0.0976580
Q4-U3R5		0.0021279	0.0252207	0.0816849	0.0962207	0.0975028	
Q4-LIM		0.073455	0.091799	0.096216	0.097299	0.097569	
Q9-U3		0.0560415	0.0962369	0.0976332	0.0976575		
Q4-U2		0.0000026	0.0000502	0.0008634	0.0121891	0.0659465	
Q4-U3		0.0000065	0.0002305	0.0054419	0.0120170	0.0537687	
Q4-U3R5	10000	0.0000219	0.0003574	0.0060313	0.0494853	0.0919406	0.0976563
Q4-LIM		0.073453	0.091797	0.096214	0.097297	0.097567	
Q9-U3		0.0013335	0.0441348	0.0961874	0.0976279		

Looking at the results from Table 7 and diagrams in Fig. 8, the best performance of the presented elements can be again noticed for the refined cubic element *Q4-U3R5*. It is notable that all pure displacement elements suffer from a locking phenomenon when applied to very thin plates modelled by coarse meshes. On the contrary, the mixed element *Q4-LIM* is insensitive to the ratio of span to plate thickness, with the exception for the very thick model, where the element

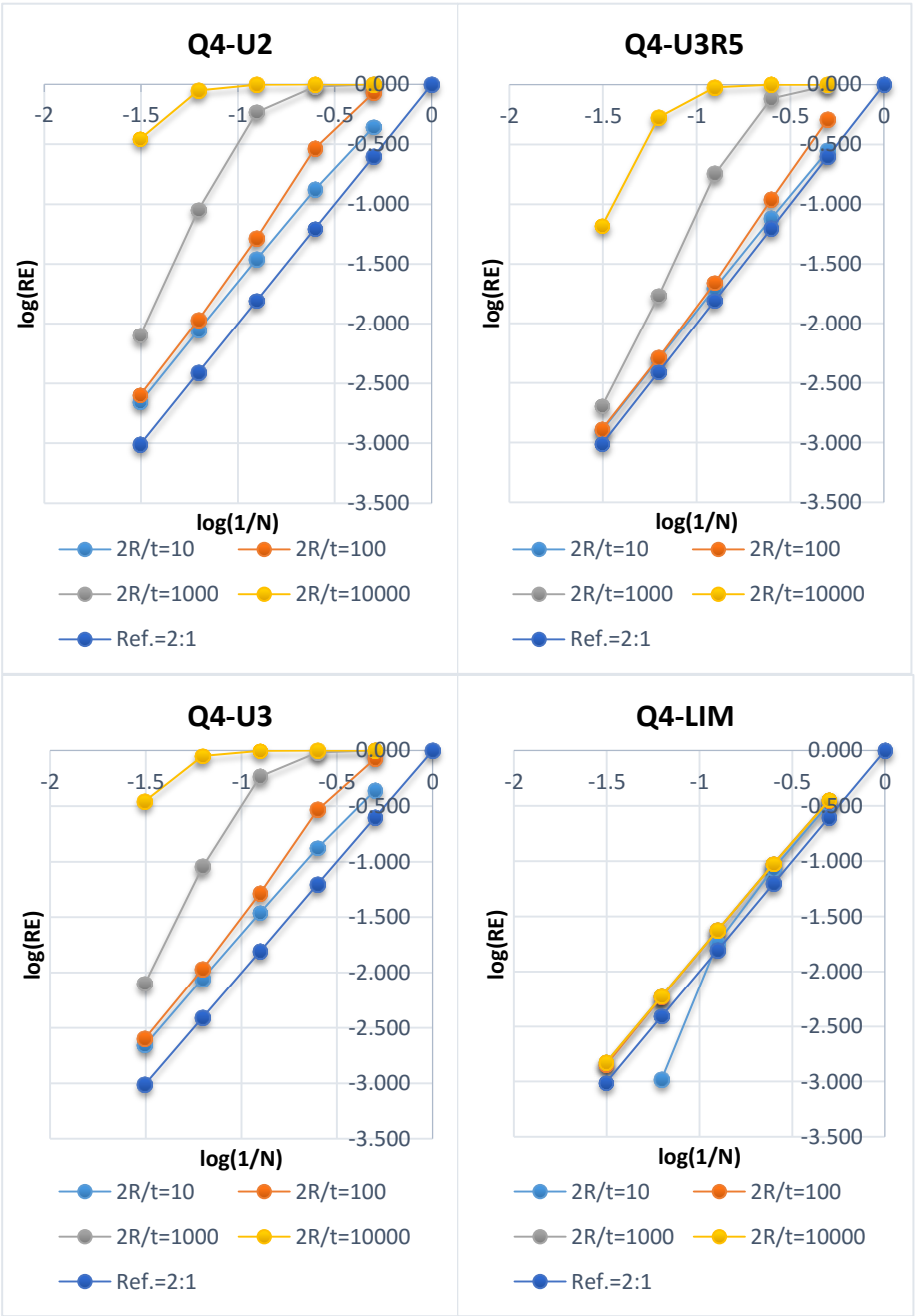

Fig. 8 Convergence curves for the circular clamped plate problem. The relative error measure is used for the analysed elements on typical meshes from Fig. 7

overestimates the analytical deformations as well as the strain energy. Slightly better performance can be noticed also for all compared elements from the literature.

4. Conclusions

In this paper the problem-dependent cubic linked interpolation for the four-node Mindlin plate finite elements is presented. In comparison with the problem-independent cubic linked interpolation implemented in *Q9-U3*, the nine-node plate element from Ribarić and Jelenić (2012), significantly less degrees of freedom are employed in the model while retaining the interpolation conformity between adjacent elements. In the problem-independent linked interpolation, the interpolation functions are independent of any problem material parameters and the rotation fields are not expressed in terms of the nodal displacement parameters. On the contrary, in the problem-dependent linked interpolation, the interpolation functions depend on the material parameters and the rotation fields are expressed in terms of the nodal displacement parameters.

Two new elements are presented, named *Q4-U3* and *Q4-U3R5*. The first one is modelled with one displacement and two rotation degrees of freedom in every of the four element nodes and the second element has five additional internal degrees of freedom which can be statically condensed within the element. Both elements are able to pass the constant-bending patch test exactly as well as the non-zero constant-shear patch test on the oriented regular mesh geometry in the case of cylindrical bending.

The locking problem exists even for the new elements applied on coarse model meshes and very thin plate models, but they behave better than *Q4-U2* (Ribarić and Jelenić 2012) although the improvement for *Q4-U3* is not substantial. On the other side *Q4-U3R5* has significantly better behavior in comparison to *Q4-U2* and in some cases is comparable to or even better than *Q9-U3* element which has as many as 12 more external degrees of freedom. A significant improvement can be noticed in particular when modeling very skew plates as well as circular plates.

The elements designed using simpler shear expressions, like the assumed shear elements, *RDKQM* (Wanji and Cheung 2000) and *ARS-Q12* (Soh *et al.* 2001) and the hybrid-Trefftz elements, *QHT* (Rezaiee-Pajand and Karkon 2012) and *HDF-P4-11β* (Cen *et al.* 2014) still behave much better in most numerical examples. By retaining only the favorable terms in the shear expressions of the *Q4-U3R5* element, a new assumed strain element may be developed, which will be investigated in future.

Acknowledgments

The results shown here have been obtained within the scientific research project IP-11-2013: 'Configuration-dependent Approximation in Non-linear Finite-element Analysis of Structures' financially supported by the Croatian Science Foundation. The University of Rijeka support for ongoing research no. 13.05.1.3.06 'Testing of Spatial slender Beam Structures with Emphasis on Model Validation' is also acknowledged.

The author would like to thank Professor Gordan Jelenić, Faculty of Civil Engineering, University of Rijeka, Croatia, for his discussions and help.

References

Auricchio, F. and Taylor, R.L. (1994), "A shear deformable plate element with an exact thin limit", *Comput. Meth. Appl. Mech. Eng.*, **118**(3), 393-412.

Bathe, K.J. and Dvorkin, E.N. (1986), "A formulation of general shell elements-the use of mixed interpolation of tensorial components", *Int. J. Numer. Meth. Eng.*, **22**(3), 697-722.

Cen, S., Shang, Y., Li, C.F. and Li, H.G. (2014), "Hybrid displacement function element method: a simple hybrid-Trefftz stress element method for analysis of Mindlin-Reissner plate", *Int. J. Numer. Meth. Eng.*, **98**(3), 203-234.

Chen, W.J., Wang, J.Z. and Zhao, J. (2009), "Functions for patch test in finite element analysis of the Mindlin plate and the thin cylindrical shell", *Sci. China Ser. G: Phys. Mech. Astron.*, **52**(5), 762-767.

Choo, Y.S., Choi, N. and Lee, B.C. (2010), "A new hybrid-Trefftz triangular and quadrilateral plate elements", *Appl. Math. Model.*, **34**(1), 14-23.

Crisfield, M.A. (1984), "A quadratic Mindlin element using shear constraints", *Comput. Struct.*, **18**(5), 833-852.

Dukić-Papa, E. and Jelenić, G. (2014), "Exact solution of 3D Timoshenko beam problem: problem-dependent formulation", *Arch. Appl. Mech.*, **84**(3), 375-384.

Hughes, T.J.R. and Tezduyar, T.E. (1981), "Finite elements based upon Mindlin plate theory with particular reference to the four-node bilinear isoparametric element", *J. Appl. Mech.*, **48**(3), 587-596.

Ibrahimbegović, A. (1993), "Quadrilateral finite elements for analysis of thick and thin plates", *Comput. Meth. Appl. Mech. Eng.*, **110**(3), 195-209.

Jelenić, G. and Papa, E. (2011), "Exact solution of 3D Timoshenko beam problem using linked interpolation of arbitrary order", *Arch. Appl. Mech.*, **81**(2), 171-183.

Lee, P.S. and Bathe, K.J. (2010), "The quadratic MITC plate and MITC shell elements in plate bending", *Adv. Eng. Softw.*, **41**(5), 712-728.

MacNeal, R.H. (1982), "Derivation of element stiffness matrices by assumed strain distributions", *Nucl. Eng. Des.*, **70**(1), 3-12.

Papadopoulos, P. and Taylor, R.L. (1990), "A triangular element based on Reissner-Mindlin plate theory", *Int. J. Numer. Meth. Eng.*, **30**(5), 1029-1049.

Rezaiee-Pajand, M. and Karkon, M. (2012), "Two efficient hybrid-Trefftz elements for plate bending analysis", *Latin Am. J. Solid. Struct.*, **9**(1), 43-67.

Ribarić, D. (2012), "Higher-order linked interpolation in moderately thick plate and facet shell finite elements", PhD Thesis, Faculty of Civil Engineering, University of Rijeka.

Ribarić, D. and Jelenić, G. (2012), "Higher-order linked interpolation in quadrilateral thick plate finite elements", *Finite Elem. Anal. Des.*, **51**, 67-80.

Ribarić, D. and Jelenić, G. (2014), "Distortion-immune nine-node displacement-based quadrilateral thick plate finite elements that satisfy constant-bending patch test", *Int. J. Numer. Meth. Eng.*, **98**(7), 492-517.

Soh, A.K., Cen, S., Long, Y.Q. and Long, Z.F. (2001), "A new twelve DOF quadrilateral element for analysis of thick and thin plates", *Eur. J. Mech. A/Solid.*, **20**(2), 299-326.

Taylor, R.L. and Auricchio, F. (1993), "Linked interpolation for Reissner-Mindlin plate elements: Part II-a simple triangle", *Int. J. Numer. Meth. Eng.*, **36**(18), 3057-3066.

Tessler, A. and Dong, S.B. (1981), "On a hierarchy of conforming Timoshenko beam elements", *Comput. Struct.*, **14**(3), 335-344.

Tessler, A. and Hughes, T.J.R. (1983), "An improved treatment of transverse shear in the Mindlin-type four-node quadrilateral element", *Comput. Meth. Appl. Mech. Eng.*, **39**(3), 311-335.

Wang, C.M., Reddy, J.N. and Lee, K.H. (2000), *Shear deformable beams and plates: Relationships with classical solutions*, Elsevier.

WanJi, C. and Cheung, Y.K. (2000), "Refined quadrilateral element based on Mindlin/Reissner plate theory" *Int. J. Numer. Meth. Eng.*, **47**(1-3), 605-627.

Xu, Z., Zienkiewicz, O.C. and Zeng L.F. (1994), "Linked interpolation for Reissner-Mindlin plate elements: Part III-An alternative quadrilateral", *Int. J. Numer. Meth. Eng.*, **37**(9), 1437-1443.

Zhang, H. and Kuang, J.S. (2007), "Eight-node Reissner-Mindlin plate element based on boundary interpolation using Timoshenko beam function", *Int. J. Numer. Meth. Eng.*, **69**(7), 1345-1373.

Zienkiewicz, O.C. and Taylor, R.L. (2000), *The finite element method: Solid mechanics*, Fifth Edition,

Butterworth-Heinemann.
Zienkiewicz, O.C., Xu, Z., Zeng, L.F., Samuelsson, A. and Wiberg, N.E. (1993), "Linked interpolation for Reissner-Mindlin plate elements: Part I-A simple quadrilateral", *Int. J. Numer. Meth. Eng.*, **36**(18), 3043-3056.

PL

Appendix A. Straight Timoshenko beam

Here we derive the solution of differential equations for the Timoshenko beam element in 2D plane depicted in Fig. 9. The beam element has the length L, constant bending rigidity EI_y (around the out-of-plane y direction) and constant shear regidity GkA. The reference coordinates are x, along the element axis and z, in the transverse direction.

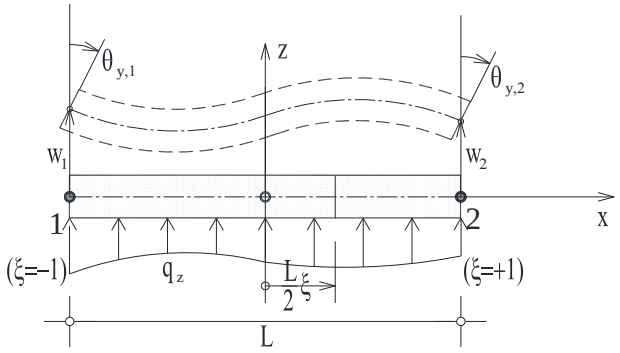

Fig. 9 Two-node straight beam element loaded in z direction.

The equilibrium equations for the diferential segment of the beam are (Jelenić and Papa 2011)

$$\sum Z = 0: \quad \frac{dV}{dx} = -q_z\,, \tag{A1}$$

$$\sum M_y = 0: \quad \frac{dM_B}{dx} - V = 0\,, \tag{A2}$$

where V and M_B are the stress resultants (shear force, section bending moment). Kinematic and constitutive equations are

$$\gamma_{zx} = \frac{dw}{dx} + \theta_y \tag{A3}$$

$$\gamma_{zx} = \frac{V}{GkA}\,, \tag{A4}$$

$$\kappa_y = \frac{d\theta_y}{dx}\,, \tag{A5}$$

$$\kappa_y = \frac{M_B}{EI_y}\,, \tag{A6}$$

where γ_{zx} denotes a shear strain and κ_y a bending curvature.

The two-node beam element is considered, assuming the four nodal degrees of freedom are

known (transverse displacements w_1 and w_2, and section rotations $\theta_{y,1}$ and $\theta_{y,2}$ at each end of the element). In the following expressions, the local position variable x measured from the beam midpoint can be replaced by a natural co-ordinate ξ such that $x = \frac{L}{2}\xi$.

The state with no distributed load along the beam segment ($q_z = 0 \Rightarrow V = V_0 = const.$) is now considered (the homogeneous part of differential equation (A1)) in more detail. Substituting the kinematic equations in the constitutive equations and the result in the equilibrium equations, gives the following differential equations of equilibrium in terms of the unknown displacement and rotation fields

$$\frac{d^3\theta_y}{dx^3} = -\frac{q_z}{EI_B} = 0, \tag{A7}$$

$$\frac{dw}{dx} = \frac{V_0}{GkA} - \theta_y. \tag{A8}$$

For q_z=0, differential Eqs. (A7) and (A8) have the following general solution

$$\theta_y = C_1\frac{x^2}{2} + C_2 x + C_3 \tag{A9}$$

$$w = -C_1\frac{x^3}{6} - C_2\frac{x^2}{2} + \left(-C_3 + \frac{V_0}{GkA}\right)\cdot x + C_4. \tag{A10}$$

For some known kinematic boundary conditions for the node 1 and together with the transformation to the natural co-ordinates we can express the nodal values in (A9) and (A10) as

$$\theta_{y,1} = C_1\frac{L^2}{8} - C_2\frac{L}{2} + C_3,$$

$$w_1 = C_1\frac{L^3}{48} - C_2\frac{L^2}{8} - \left(-C_3 + \frac{V_0}{GkA}\right)\cdot\frac{L}{2} + C_4$$

and similarly for the node 2:

$$\theta_{y,2} = C_1\frac{L^2}{8} + C_2\frac{L}{2} + C_3,$$

$$w_2 = -C_1\frac{L^3}{48} - C_2\frac{L^2}{8} + \left(-C_3 + \frac{V_0}{GkA}\right)\cdot\frac{L}{2} + C_4.$$

Now the integration constants can be expressed in terms of the nodal boundary displacements and rotations as

$$C_2 = \frac{\theta_{y,2} - \theta_{y,1}}{L},\ C_3 = \frac{\theta_{y,1} + \theta_{y,2}}{2} - \frac{V_0}{EI_B}\frac{L^2}{8},\qquad C_4 = \frac{w_1 + w_2}{2} + \frac{\theta_{y,2} - \theta_{y,1}}{4}\frac{L}{2},\qquad C_1 = \frac{V_0}{EI_B}$$

and also the constant V_0 can be expressed from (A3) and (A4) as

$$V_0 = \frac{\dfrac{w_2 - w_1}{L} + \dfrac{\theta_{y,1} + \theta_{y,2}}{2}}{\dfrac{L^2}{12EI_B} + \dfrac{1}{GkA}}. \tag{A11}$$

Using (A9) and (A10), there follows

$$\theta_y = \frac{\theta_{y,1} + \theta_{y,2}}{2} + \frac{\theta_{y,2} - \theta_{y,1}}{2}\xi - \frac{\dfrac{L^2}{12EI_B}}{\dfrac{L^2}{12EI_B} + \dfrac{1}{GkA}}\left(\frac{w_2 - w_1}{L} + \frac{\theta_{y,1} + \theta_{y,2}}{2}\right)\frac{3}{2}\left(1 - \xi^2\right),$$

i.e.

$$\theta_y = \theta_{y,2N} + \Delta\kappa_{12} \cdot L\frac{\left(1 - \xi^2\right)}{4} \tag{A12}$$

and

$$w = \frac{w_1 + w_2}{2} + \frac{w_2 - w_1}{2}\xi + \frac{\theta_{y,2} - \theta_{y,1}}{2}\frac{L}{4}\left(1 - \xi^2\right) + \frac{\dfrac{L^2}{12EI_B}}{\dfrac{L^2}{12EI_B} + \dfrac{1}{GkA}}\left(\frac{w_2 - w_1}{L} + \frac{\theta_{y,1} + \theta_{y,2}}{2}\right)\frac{L}{4}\xi\left(1 - \xi^2\right)$$

i.e.

$$w = w_{2L} - \Delta\kappa_{12}\frac{L^2}{6}\frac{\xi\left(1 - \xi^2\right)}{4} \tag{A13}$$

where $\theta_{y,2N}$ is the standard two-node Lagrangian interpolation for θ_y and w_{2L} is the two-node (quadratic) linked interpolation for w and

$$\Delta\kappa_{12} = \frac{-1}{1 + \dfrac{12EI_B}{GkAL^2}}\left(\frac{w_2 - w_1}{L} + \frac{\theta_{y,1} + \theta_{y,2}}{2}\right)\frac{6}{L} \tag{A14}$$

is a curvature increment between nodes 1 and 2.

Using (A5) and (A6) gives

$$M_B = EI_B\left(\frac{\theta_{y,2} - \theta_{y,1}}{L} - \Delta\kappa_{12} \cdot \xi\right). \tag{A15}$$

Furthermore from (A2) and (A15) expression for shear force follows, which has already been derived in (A11)

$$V_0 = -EI_B\frac{2}{L}\Delta\kappa_{12}. \tag{A16}$$

Eqs. (A12) and (A13) show that the unknown fields are expressed not only through the

independent natural co-ordinate and their nodal values but also by the material properties of the problem analysed (EI_B, GkA) in the highest-order polynomial terms. In Dukić and Jelenić (2014) this type of linked interpolation was named *problem-dependent*.

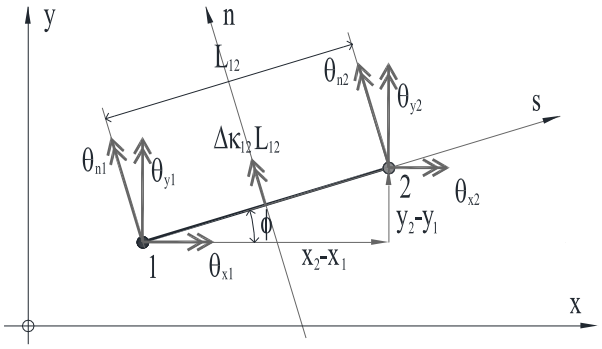

Fig. 10 Two-node straight beam element with general orientation in *x*-*y* plane and loaded in *z* direction

Assuming a more general orientation of the beam (Fig. 10), in which it still remained subject to the force loading in the direction of the co-ordinate axis *z* and the moment loading around an axis orthogonal to the beam axis (a new axis of the beam lying in the co-ordinate plane *x*-*y*, closing an angle $\boldsymbol{\varphi}$ with respect to the co-ordinate axis *x*), the cross-sectional rotation θ_y in the above expressions would only need to be replaced by a new normal rotation $\theta_n=\theta_y\cos\varphi-\theta_x\sin\varphi$ of which the componential rotations around the co-ordinate axis would be $\theta_x=-\theta_n\sin\varphi$ and $\theta_y=\theta_n\cos\varphi$**.** Clearly, above expressions (A12) and (A13) would then turn into

$$\theta_x = \theta_{x,2N} - \Delta\kappa_{12}\sin\varphi\cdot L\frac{\left(1-\xi^2\right)}{4}, \tag{A17}$$

$$\theta_y = \theta_{y,2N} + \Delta\kappa_{12}\cos\varphi\cdot L\frac{\left(1-\xi^2\right)}{4}, \tag{A18}$$

$$w = w_{2L} - \Delta\kappa_{12}\frac{L^2}{6}\cdot\frac{\xi\left(1-\xi^2\right)}{4}, \tag{A19}$$

with $\Delta\kappa_{12}=\dfrac{-1}{1+\dfrac{12EI_B}{GkAL^2}}\left(\dfrac{w_2-w_1}{L}-\dfrac{\theta_{x,1}+\theta_{x,2}}{2}\sin\varphi+\dfrac{\theta_{y,1}+\theta_{y,2}}{2}\cos\varphi\right)\dfrac{6}{L}$ and $\xi\in\left[-1,1\right]$ as the natural co-ordinate of a cross-section position.